INT. J. REMOTE SENSING, 1996, VOL. 17, NO. 12, 2259–2280

Extraction of the pure spectral response of the landscape components in NOAA-AVHRR mixed pixels—application to the HAPEX-Sahel degree square

H. OUAIDRARI†, A. BÉGUÉ‡, J. IMBERNON§

CIRAD-CA, Maison de la Télédétection, 500 rue J. F. Breton, 34 093 Montpellier Cedex 5, France

and J. M. D'HERBES

ORSTOM, Maison de la Télédétection, 500 rue J. F. Breton, 34 093 Montpellier Cedex 5, France

(*Received 31 July 1995; in final form 31 January 1996*)

Abstract. A method to estimate the pure reflectance of landscape components in mixed pixels is presented in this paper. Based on the usual linear mixture model, this original method allowed us to restitute the temporal and spatial variability of the reflectance of the components of a NOAA-AVHRR scene. Ground cover proportions were obtained from a SPOT image classification degraded at NOAA resolution. The signal deconvolution was made using blocks of pixels to limit the errors due to the misregistration between NOAA and the ground cover images. The model was applied to NOAA-AVHRR simulations and to actual NOAA temporal series (1992) over the HAPEX-Sahel degree square, to deconvoluate the reflectances of the three landscape components (millet, fallow and plateau). The data analysis indicated a high sensitivity of the method to the misregistration and the need to define an optimal size of pixels which provide a good compromise between the misregistration errors and the spatial variability of the reflectance components. The deconvoluated reflectances were compared to airborne measurements acquired over two sites during the HAPEX-Sahel experiment. The quality of the results depends on the type of landscape. The model performs best on a landscape with small surface units, well spatially distributed.

1. Introduction

Additionally to spatial information, satellite remote sensing provides temporal information on the spectral characteristics of the surface components. Coarse resolution satellites, such as the National Oceanograph and Atmospheric Administration (NOAA) series (1·1 km nadir), provide theoretically one to two images per day. Even for regions with high cloud coverage, this temporal resolution permits correct vegetation monitoring at a regional scale (e.g. Tucker *et al.* 1985, Justice 1986, Malingreau 1986). However, at coarse resolution the size of the ground viewed in an image pixel is generally larger than the size of the surface units. In that case, the image pixel is composed by a mixture of surface components and is generally referred to as a 'mixed pixel', in opposition to a 'pure pixel' composed of a single component. Mixed

†Present address: NASA/GSFC, Code 923, Greenbelt, MD 20771, U.S.A.
‡Corresponding author.
§Present address: ICRAF, United Nations Av., PO Box 30677, Nairobi, Kenya.

0143–1161/96 $12.00

pixels are a strong limitation for the use of coarse resolution satellite in vegetation monitoring. In effect, it is important to be able to isolate the spectral characteristics of a particular canopy either to detect directly any climatic accident by analysing change in the seasonal shape, or to derive biophysical parameters to be used in primary production modelling.

In some cases, the problem of mixed pixel can be dodged. Guérif *et al.* (1991) used SPOT images classification over Algeria to detect NOAA pixels where cereals are dominant. The seasonal response of these selected pixels was then used in a model of biomass and yield estimation. Disregarding the particular feature of the landscape, the representativity of the selected pixels for the whole scene is not straight forward.

Generally, mixing problems are treated in remote sensing by linear mixture modelling. It is a simple mathematical description of the generation of a mixture signal, and seems to be appropriate for many land-based scenes. At coarse resolution, the linear mixture model is often used to estimate the ground cover proportions provided the spectral response of the components obtained from NOAA training pixels (e.g., Quarmby *et al.* 1992), principal components feature space (e.g., Cross *et al.* 1991), laboratory measurements (e.g., Smith *et al.* 1987) or high resolution images calibrated by linear regression (e.g., Holben and Shimabukuro 1993, Kerdiles and Grondona 1995). Few people have used it to estimate the spectral response of the components providing the ground cover proportions (Hanan *et al.* 1991).

In the south-west of France, where the landscape is a patchwork of small size fields, Puyou-Lascassies *et al.* (1994) realized a theoretical study on coarse resolution signal deconvolution in order to establish eight profiles of vegetation indices. Land use data came from SPOT and Landsat image classification, and coarse resolution data (1·21 km^2) were obtained by degradation of those same high spatial resolution images. The linear mixing model was solved by multiple linear regression over the whole image. This method gives very good results, but seems to be very sensitive to the misregistration between the classification and the coarse resolution images (personal communication). This statistical method has been applied successfully on actual NOAA-Advanced Very High Resolution Radiometer (AVHRR) time series over Yatenga province in Burkina-Faso (Cherchali and Flouzat 1994) and over the First International Satellite Land Surface Climatology Project (ISLSCP) Field Experiment (FIFE) site in Kansas (Oleson *et al.* 1995). Unfortunately no details are given in these studies on the sensitivity of the method to the misregistration between NOAA images and the land cover classifications issued from high-resolution satellite images.

Fischer (1994) developed a semi-empirical model to represent the temporal variations of a vegetation index, based on the use of a double logistic function (five parameters) to describe the temporal evolution of the vegetation index of a pure crop. The model parameters are then retrieved through a nonlinear least square fitting. This method has been applied to AVHRR data over the Beauce region (France), and provides good profiles of Normalized Difference Vegetation Index (NDVI) for the winter and summer crops. This method is adapted to time differenciated crops having a regular growth.

These examples show that the mixed pixel problem is treated differently according to the landscape. In semi-arid regions, the size of the fields, the high variability of the spectral characteristics of a crop at a regional scale, a short growing season and the risk of climatic accident throughout the growing period prevent the use of most of the existing methods. A new methodology based on linear mixture modelling and

adapted to semi-arid regions is therefore proposed in this paper. This methodology takes into account, and tends to restitute, the spatial variability of the reflectance of the landscape components.

This study takes advantage of the HAPEX-Sahel experiment at (Goutorbe *et al.* 1994) results. The study area, a 1° by 1° square centred on Niamey (Niger), has been classified from SPOT imagery to produce a soil surface conditions map. This map provides information on the ground cover of the main components of the landscape. In this paper, the study area is first presented, and the linear mixture model and its application to NOAA images is described. Pure reflectance of the components is then extracted from 1992 NOAA-AVHRR images of the degree square, and compared to airborne radiometric measurements performed over 2 HAPEX-Sahel sites throughout the growing season.

2. Study area and ground data

2.1. *HAPEX-Sahel degree square*

HAPEX-Sahel (Hydrologic Atmospheric Pilot Experiment in the Sahel) took place in Niger (West Africa) during 1991–1992, in order to improve the parameterization of land surface atmosphere interactions at the General Circulation Model (GCM) grid-box scale (Goutorbe *et al.* 1994). The experiment was based on a 1° by 1° square (2–3° E, 13–14° N), that contains Niamey (figure 1).

Mean rainfall at Niamey is about 560 mm (1905–1989), with a north to south gradient of about 1 mm km^{-1} (Lebel *et al.* 1992). The rainy season is generally from June to September.

The area contains reasonable examples of the more widespread surfaces that can be found in the Sahel (Prince *et al.* 1995). There are three main vegetation types: arable crops (almost entirely millet), fallow savannah and tiger-bush. The areas of millet (*Pennisetum glaucum* (L.) R.Br.) are sown in clumps at the beginning of the rainy season. The fallow savannah contains diverse mixtures of naturally occurring perennial woody shrubs (*Guiera senegalensis* (L.) is dominant over the degree square) and herbaceous annual plants. The tiger-bush only occurs on the laterite plateaux, and is made of dense strips of vegetation (trees) separated by areas of completely bare soil. According to the rainfall, the density of the vegetation decreases from south to north.

2.2. *Vegetation map*

A map of soil surface conditions of the HAPEX-Sahel degree square has been made from a supervised classification of a mosaic of 6 SPOT images taken on 24 October 1988 (d'Herbes *et al.* 1992). This cartography includes geomorphological, vegetation, pedological and hydrological features of the landscape. It results in a 12 classes map, whose legend is given in table 1.

In order to reduce the information to a vegetation map, the original 12 classes have been reduced to three classes whose correspondances are given in table 1 (Prince *et al.* 1995):

- The 'plateau' class regroups the plateaus, the sand covered plateaus and the plateau edges. It represents about 21 per cent of the degree square area.
- The 'millet' class regroups the agriculture lands and half of the agro-pastoral lands. This class covers about 52 per cent of the area.

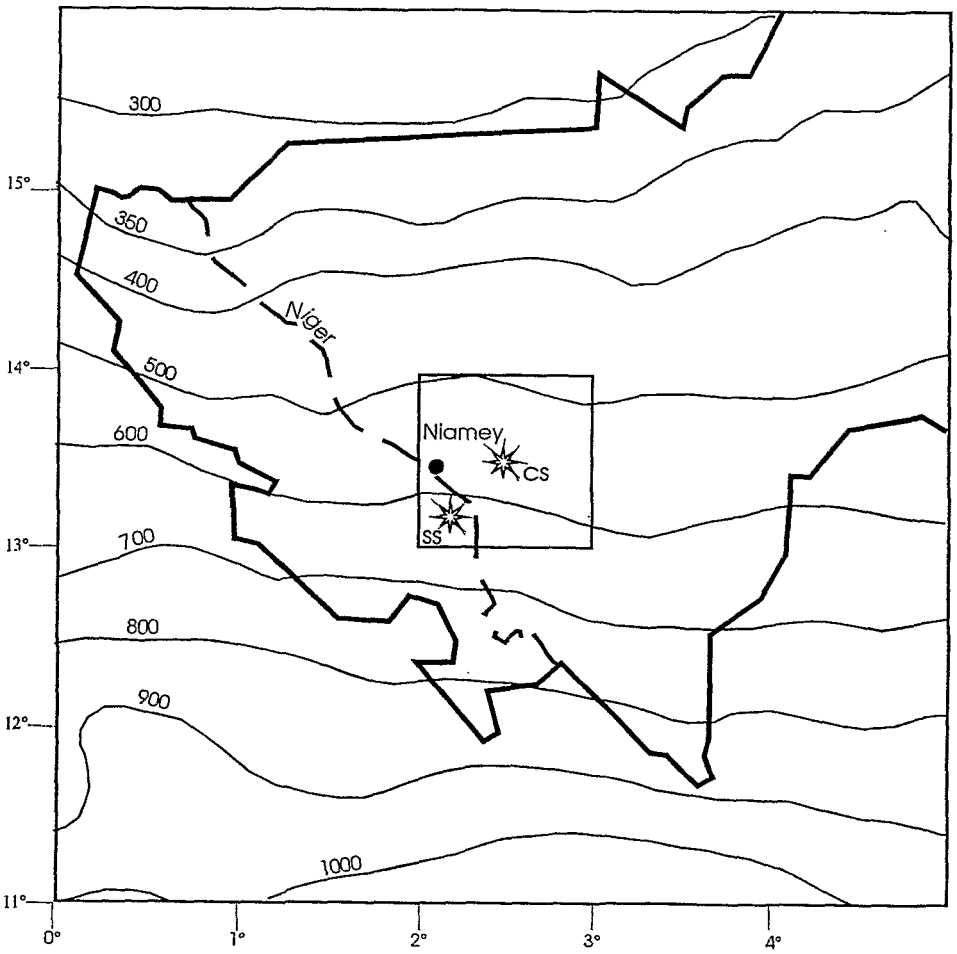

Figure 1. Location of the HAPEX-Sahel degree square in Western Niger and location of the Central (CS) and South (SS) sites. The isohyets represent the mean annual rainfall on the 1951–1980 period (AGRHYMET 1992).

- The 'fallow' class regroups the fallow lands, half of the agro-pastoral lands and the dry forests. This class covers about 27 per cent of the area.

The resulting three classes map is shown in figure 2.

2.3. *Radiometric measurements*

Three supersites were identified inside the HAPEX-Sahel degree square, each approximately 20 km × 20 km (figure 1). The two central supersites are made of small size plateau separated by agro-pastoral areas, while the Southern supersite is composed of a large size plateau, north–south oriented. During the 1992 field experiment, measurements of surface reflectances in the visible and near-infrared have been made from low altitude light aircraft transects over these supersites (Hanan *et al.* 1996) Radiances were measured in the Thematic Mapper bands (TM3: 630–690 nm and TM4: 760–900 nm) with an Exotech 100AX radiometer at nadir. The nominal field of view of the radiometer was 52·7 m diameter. The measurements were generally

Table 1. The legend of the spatio-map of the soil surface conditions (d'Herbes *et al.* 1992) and land units of the HAPEX-Sahel degree square.

Original class	Dominant characteristic	Vegetation cover	Principal land use	Area (ha)	Grouping class*
1	Plateau edge	None-low	Sylvo-pastoral	16 170	P
2	Plateau	None	None	54 590	P
3	Plateau	None	None	92 320	P
4	Sand covered plateau	None-low	Agro-sylvo-pastoral	90 280	P
5	Azonal	—	Agriculture and urban	128 200	M
6	Aeolian sand	Medium-dense	Fallow	63 300	F
7	Azonal	Dense	Forest and rice	70 370	F
8	Aeolian sand	None-medium	Agro-pastoral	185 420	0·5 M+0·5 F
9	Aeolian sand	None-low	Agriculture	155 920	M
10	Valley bottoms, sandy plains	None-medium	Agro-pastoral	235 000	0·5 M+0·5 F
11	Azonal	Low-medium	Agro-pastoral	88 600	0·5 M+0·5 F
12	Open water	—	—	6100	—

*P for plateau, M for millet and F for fallow.

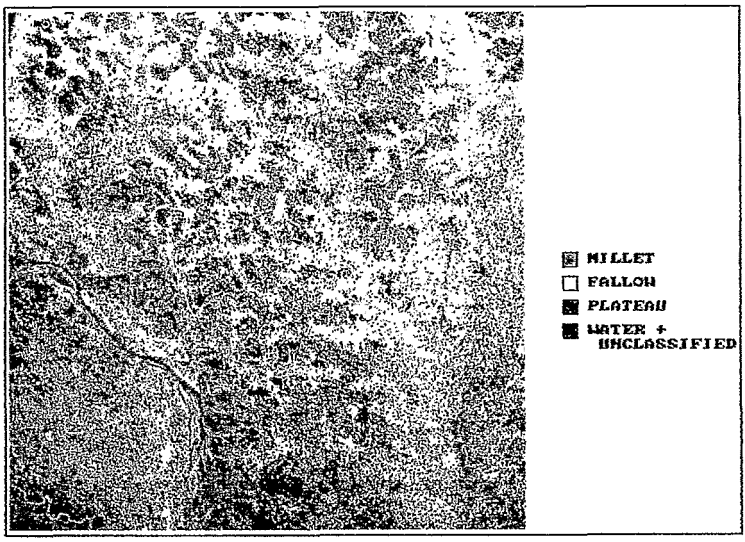

Figure 2.

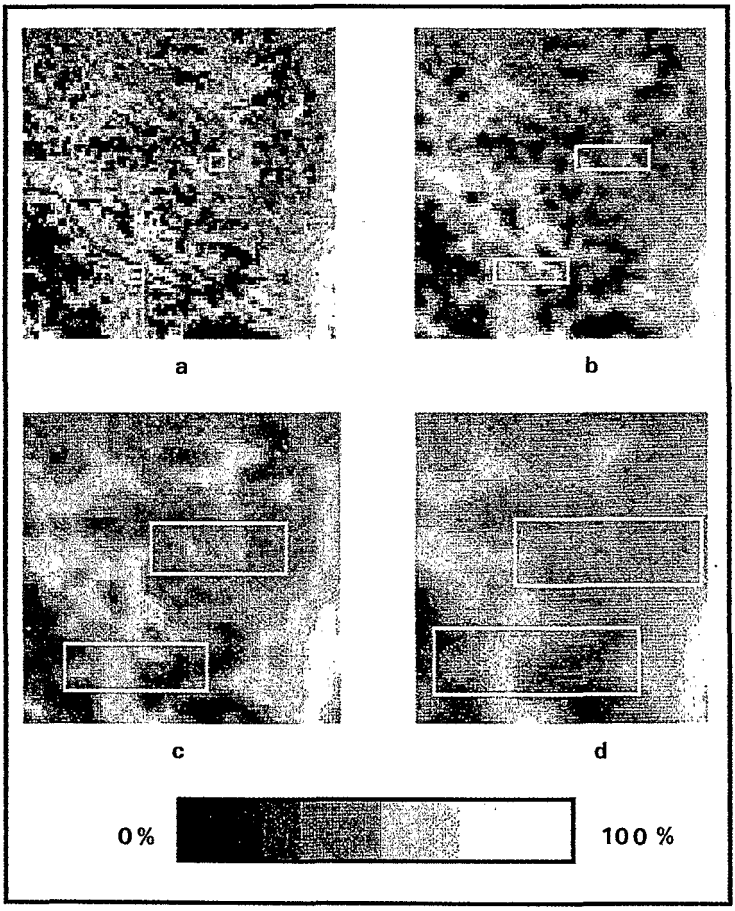

Figure 5.

made in the morning, around 10 am. During aircraft measurements, incident visible and near-infrared radiation were continuously measured in the fields using another Exotech radiometer viewing a calibrated reflectance panel. These data were used to estimate surface reflectances from the aircraft measured surface radiances.

To test the deconvolution method proposed in this paper, two sites have been selected (figure 1). One is located within the West-Central supersite (13° 30′ N–2° 28′ E), the other is located within the Southern supersite (13° 11′ N–2° 19′ E). These sites are referred to in this paper as the Central site (CS) and the South site (SS) respectively.

3. Method

3.1. *Linear mixture model*

The basic physical assumption underlying the linear mixing model is that there is no significant amount of multiple scattering between the different cover types, so that the signal measured by a sensor can be considered as the sum of the signals received from each cover component weighted by their respective area. Under these conditions and for a given spectral band, the expected reflectance value R of a mixed pixel made of n ground cover components is

$$R = \sum_{i=1}^{n} P_i \rho_i . \tag{1}$$

where P_i is the proportion of surface area of the components i and ρ_i is the mean reflectance of the component i.

The linear mixture seems to be a good assumption at the scale of the Sahelian landscapes since the different cover types are large enough not to interfere. Our methodology is based on the linear mixture.

3.2. *Mixing system*

To have a unique set of solutions (ρ_i), the number of linear equations must be equal to the number of unknowns n. These n equations will be referred to as the mixing system:

$$\left.\begin{aligned} R_1 &= P_{11}\rho_1 + P_{21}\rho_2 + \ldots + P_{n1}\rho_n \\ R_2 &= P_{12}\rho_1 + P_{22}\rho_2 + \ldots + P_{n2}\rho_n \\ &\vdots \\ R_n &= P_{1n}\rho_1 + P_{2n}\rho_2 + \ldots + P_{nn}\rho_n \end{aligned}\right\} \tag{2}$$

In our case, as there are three unknowns (the reflectance of millet, the reflectance of fallow and the reflectance of plateau) the mixing system must be composed of three equations ($n=3$).

Figure 2. SPOT image classification of the HAPEX-Sahel degree square (from d'Herbes *et al.* 1992).

Figure 5. Millet fraction images calculated at four spatial resolutions: (*a*) NOAA resolution, (*b*) 3 × 3 pixels blocks, (*c*) 6 × 6 pixels blocks and (*d*) 9 × 9 pixels blocks. In (*a*), white squares indicate the location of the sites, and in (*b*), (*c*), (*d*), white lines delineate the influence zones of the Central and South sites.

3.3. *Solving the mixing systems*

In the mixing system equation (3), R represent the reflectances of a NOAA pixel made up of upto three different ground cover components. Unfortunately, the proportions of these components cannot be accurately defined at the NOAA pixel scale, because of problems of misregistration between the vegetation map and NOAA images. Therefore, we chose to solve the mixing system on blocks of pixels rather than on single pixels. The blocks are square and of reflectance equal to the mean reflectance of the pixels inside the block. The choice of the blocks size is a key point in the methodology, and will be discussed later.

Additionally to the size of the blocks, the location of the three blocks of the mixing system is important. Their spatial orientation must be driven by the gradient of the satellite image, if one exists. For instance, in our case, there is a north–south gradient in reflectances due to the gradient of rainfall. The mixing system resolution is then carried out preferentially east–west, in the direction where the radiometry of a component is likely to be homogeneous. The juxtaposition of the three blocks is referred to hereafter as a 'window' (figure 3).

The mixing system is first solved on the three blocks of a window located at the left-top corner of the image. The window is then shifted one column forward, and a new system is solved. This procedure is iterated up to the right border of the image. Then the window is shifted one line forward from the left-top corner and a new system is solved. The window is then shifted one column forward and so on, until the whole image has been explored by the sliding window. Each mixing system provides a set of reflectance for the three classes. There are about as many sets of solutions as number of pixels in the image.

During this process, each pixel participates to several mixing systems (figure 3). The number N of these system, equivalent to the number N of the windows sharing a common pixel, is the product between the number of columns (equal to the size of three blocks) and the number of lines (equal to the size of one block) shifted around this pixel, and is equal to $(3b^2)$, with b the size of the side of the square blocks expressed in pixels and referred hereafter as 'block size'. The number of mixing systems as function of the block size is plotted in figure 4.

The part of the image explored by the windows sharing a given pixel is referred to hereafter as the 'influence zone' of the pixel (figure 3). The influence zone is not square due to the juxtaposition of the three blocks. Its east–west size is $(6b-1)$ pixels and its north–south size is $(2b-1)$ pixels (figure 4).

As seen previously, each mixing system provides a set of three reflectances, one for each class. So, for a given pixel, the N mixing systems produce theorically N sets of reflectances. The 'pure' reflectance of the components of such a pixel is calculated as the average of these N reflectances (figure 3). This technique also allows for the estimation of the variability of those reflectances through the value of the ratio between the mean square error and the mean reflectance of the component.

4. Sensitivity analysis on NOAA simulations

The size of the blocks must be a compromise between the misregistration of the map and the satellite image, and the variability of the reflectance of the components over the satellite image. In effect, large blocks will decrease the sensitivity of the method to the misregistration, but will probably increase the reflectance variability inside the blocks resulting in incorrect mixing systems. To study the sensitivity of the method to the block size and to the misregistration, a sensitivity analysis is made

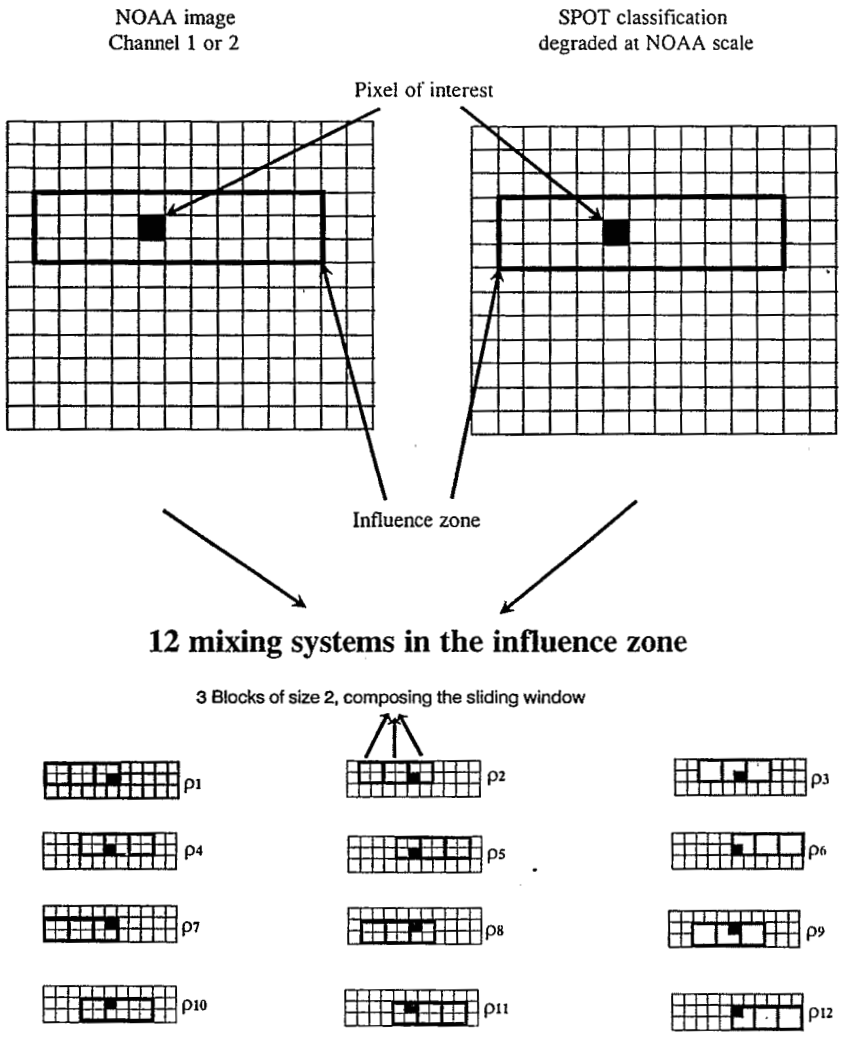

Figure 3. Sketch of the mixing system, for $b=2$. For a given component, and a given pixel—Mean reflectance: $\rho = 1/12 \sum_{i=1}^{i=12} \rho_i$, Variance: $\mathrm{Var} = 1/12 \sum_{i=1}^{i=12} (\rho_i - \rho)^2$.

on simulated coarse resolution images, where the radiometry of the mixture component is taken homogeneously over the study area. The reversibility of the model is then tested on two sites (the central and south sites) and discussed according to two criteria: the number of accepted solutions and the error committed on the calculated pure reflectance of the landscape components.

4.1. *Simulation of coarse resolution images*

Simulation of the reflectance of the coarse resolution pixel is obtained by linear mixture modelling:

- The proportions of the components are given by the fraction images obtained by degradation of the vegetation map at NOAA resolution (Justice *et al.* 1989). The millet fraction image is given in figure 5 (*a*).

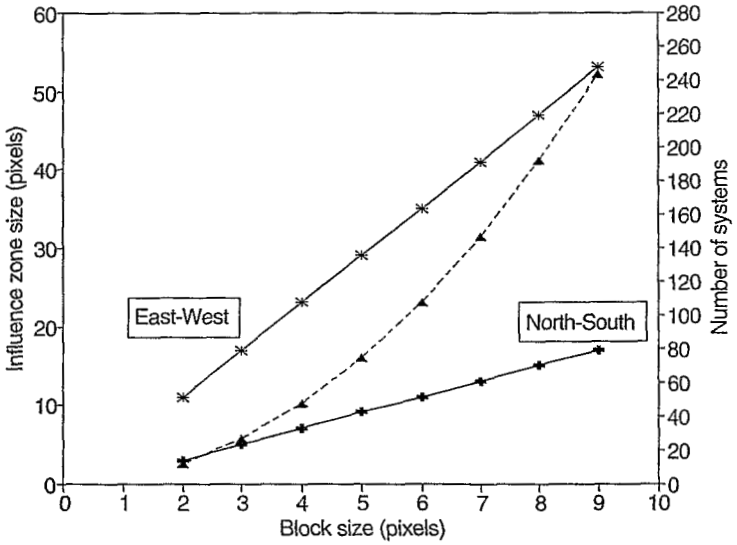

Figure 4. Sizes of the influence zone (solid lines) and number of mixing systems (dashed line), as function of the block size.

- The reflectances of the components are derived from near-infrared measurements made over the central site in the middle of the rainy season (Hanan *et al.* 1996): 0·5, 0·4 and 0·3 roughly for the millet, fallow and plateau respectively.

To study the sensitivity of the method to the block size, the NOAA fraction images are degraded at eight spatial resolutions (from 2×2 to 9×9 NOAA pixels). The example of the millet fraction images at different resolutions are given in figures 5(*a*)–(*d*). On these figures, the corresponding influence zones of the Central and South sites are delineated.

To study the sensitivity of the method to the misregistration, three geometric misregistrations are simulated by shifting forward 1, 2 or 3 columns of the fraction images.

4.2. *Number of accepted solutions*

As seen previously, N mixing systems give theorically N sets of reflectances. In practice, only the solutions with reflectances within the zero one interval are accepted and used to calculate the pure reflectance of the components. The mixing systems can give impossible solutions either if the equations are identical or if the fractions of components are false. In the case of a natural landscape, with no geometrical pattern, the equations are unlikely to be identical. This is illustrated by the 100 per cent of accepted solutions on the Central and South sites when there is no misregistration (figure 6). The rejected solutions are only due to false cover proportions.

The modification in ground cover easily explains why the proportion of accepted solutions decreases with the number of misregistered pixels and increases with the size of the blocks (figure 6). In effect, a given shift of columns will less affect the components proportions within the area of a large block of pixels than within the area of a small one. For block size smaller than 4, the number of accepted solutions

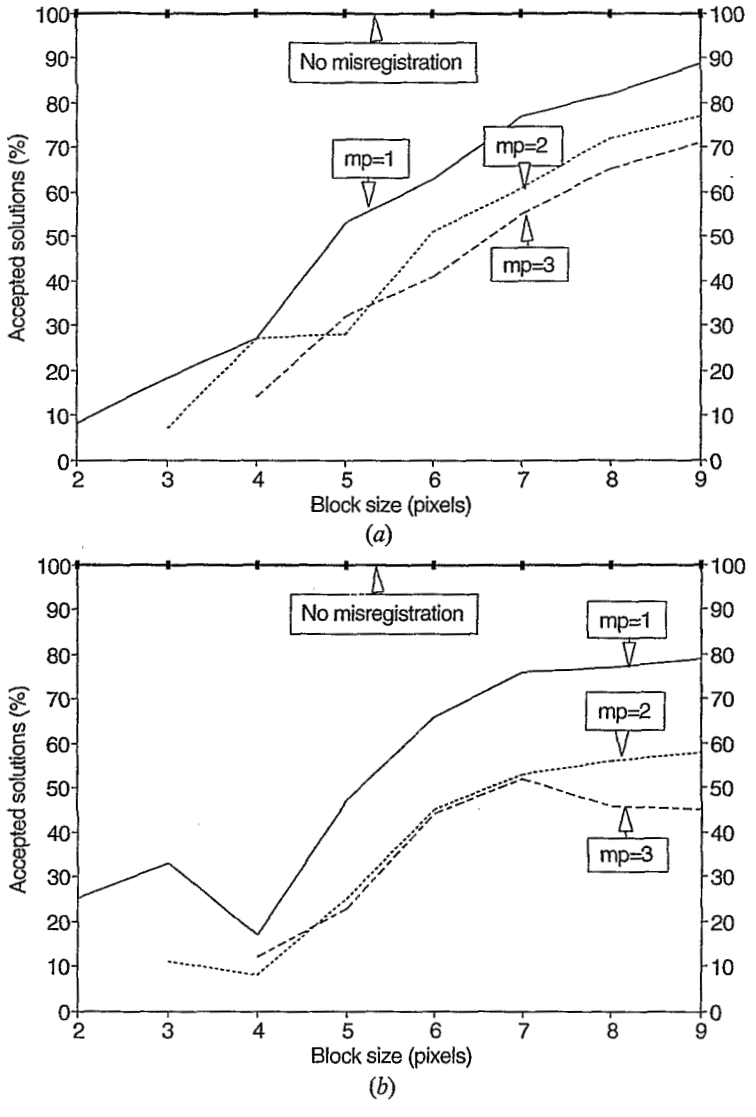

Figure 6. Proportions of accepted solutions of the mixing systems in function of the block size and the number of misregistered pixels (mp) for (*a*) the Central site, and (*b*) the South site.

corresponds to less than nine mixing systems and therefore will not be considered in the following discussion.

The differences between CS (figure 6(*a*)) and SS (figure 6(*b*)) are rich in information. The proportion of accepted solutions of CS increases almost monotically with the size of the blocks (up to 90 per cent of accepted solutions for one misregistered pixel and above 70 per cent for more misregistration), while for SS this proportion is almost stationary for block sizes above seven pixels and reaches only 80 per cent for one misregistered pixel and less than 60 per cent for more misregistration. These differences can be explained by the landscape pattern inside the influence zones of the sites (figure 7). On CS (figure 7(*a*)), the proportion of fallow is constant whatever

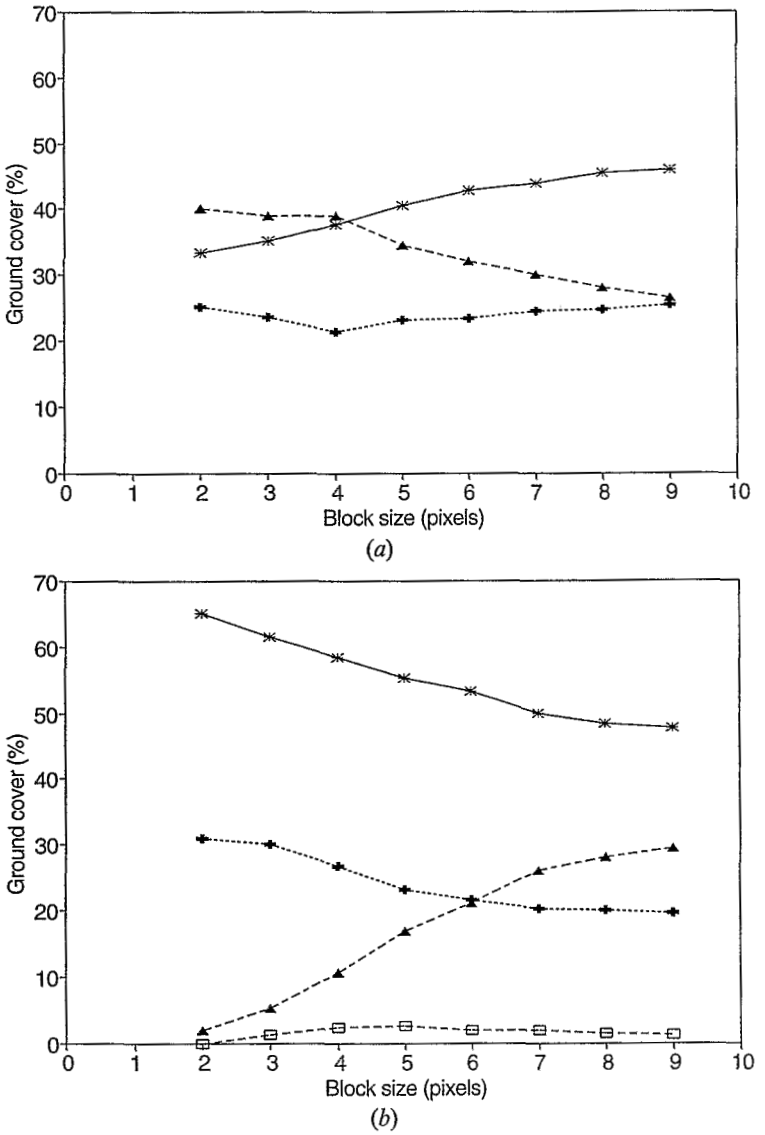

Figure 7. Proportions of millet (solid line), fallow (dotted line), plateau (dashed line) and unclassified (square symbols) pixels as function of the block size, in the influence zone of (*a*) Central, and (*b*) South sites.

the block size (around 25 per cent), and the proportions of millet and plateau varies a little (around 10 per cent of change between a block size of 2–9). Additionally to small changes in proportions, the landscape units are relatively small and spatially well distributed (figure 5). In that case, a shift of column does not modify dramatically the composition of the landscape, and the number of accepted solutions is acceptable. On SS (figure 7(*b*)), the proportions of the components change a lot with the block size, as illustrated by the proportion of plateau almost zero at small block sizes and reaching 30 per cent at a block size of 9. With the increase of block size, the influence

zone of SS includes large and contrasted units of plateau which makes the mixing systems more sensitive to the misregistration.

4.3. *Error on the calculated pure reflectance*

Table 2 presents the errors made on the calculated pure reflectance of CS and SS landscape components. This error is the difference between calculated and theoretical reflectances, normalized by the theoretical reflectance (constant over the whole image, for memory). It is a good indicator of the sensitivity of the methodology to the misregistration and the size of the blocks. As expected, the errors tend to decrease with the size of the blocks and to increase with the number of misregistered pixels. On CS, the calculated reflectances are in the same range than theoretical reflectances for one pixel of misregistration. For higher misregistration, the response of the millet and the fallow are not correctly restitued. On SS, there is a slight confusion between millet and fallow. This result must be related to the previous conclusions on the number of accepted solutions.

Table 2. Relative error (%) on the calculated pure reflectance of the Central and South sites landscapes components, in function of the block size and the number of misregistered columns.

			Block sizes *b* (pixels)					
Site			4	5	6	7	8	9
Central site	Millet	0*	0	0	0	0	0	0
		1	8	10	2	8	6	6
		2	28	18	4	12	8	6
		3	18	22	26	14	14	10
	Fallow	0	0	0	0	0	0	0
		1	5	18	5	10	13	8
		2	13	25	18	18	18	15
		3	13	33	30	23	25	18
	Plateau	0	0	0	0	0	0	0
		1	10	3	3	0	0	0
		2	33	13	10	3	3	3
		3	50	13	23	7	3	7
South site	Millet	0	0	0	0	0	0	0
		1	18	14	12	14	8	6
		2	18	12	18	14	14	8
		3	8	14	20	18	16	10
	Fallow	0	0	0	0	0	0	0
		1	28	28	23	25	15	15
		2	23	15	23	18	23	18
		3	8	18	28	20	20	13
	Plataeu	0	0	0	0	0	0	0
		1	20	10	7	7	3	0
		2	20	10	13	13	10	3
		3	7	10	17	19	13	10

* Number of misregistered columns.

Another indicator of the sensitivity of the method is the coefficient of variation of the calculated reflectances. Figure 8 gives the results for one column of misregistration. Again, the general trend is a decrease with the size of the blocks, except for the fallow and the plateau of site SS which display a minimum at a block size of seven. The coefficient of variation is not very sensitive to the misregistration (table 3). This could be explained by the fact that the mixing systems with large errors in ground cover have been eliminated by the test on the calculated reflectances.

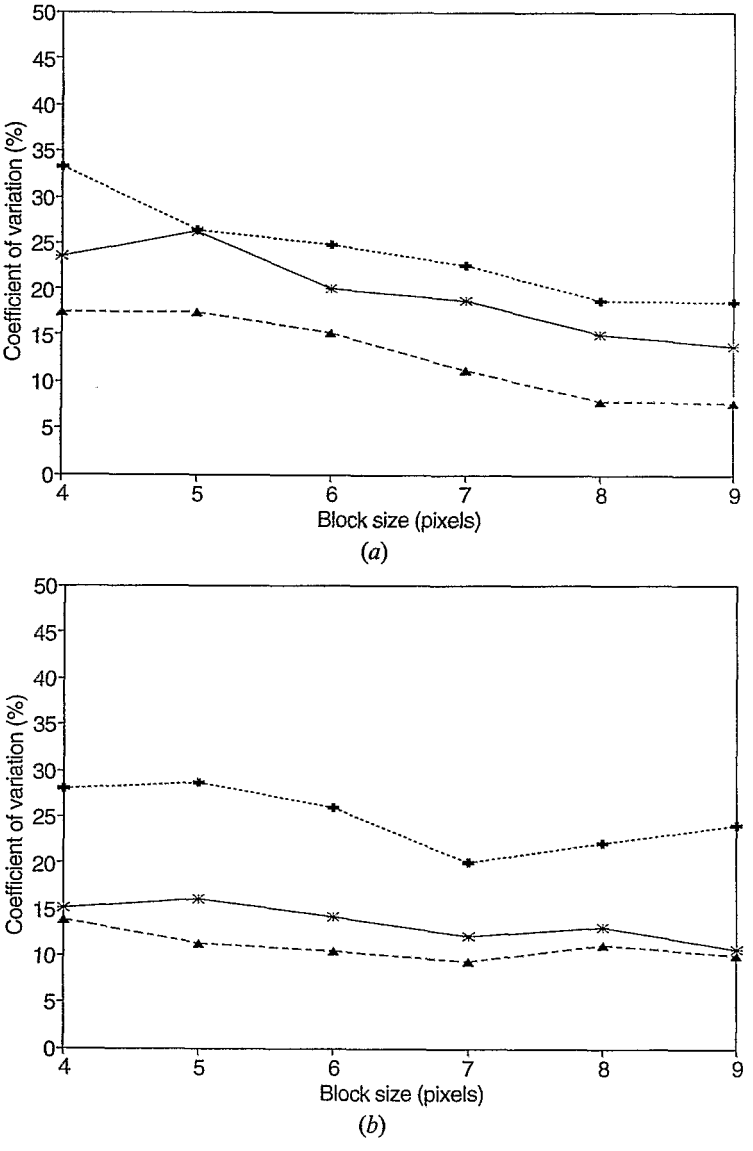

Figure 8. Coefficient of variation of the simulated near-infrared reflectances of millet (solid line), fallow (dotted line), and plateau (dashed line) components as function of the block size. Calculations were made for one column of misregistration, on the (*a*) Central, and (*b*) South sites.

Table 3. Variation coefficient (%) of the calculated pure reflectance of the Central and South sites landscapes components, in function of the block size and the number of misregistered columns.

Site			Block sizes *b* (pixels)					
			4	5	6	7	8	9
Central site	Millet	1*	24	26	20	19	15	14
		2	17	23	20	19	12	14
		3	11	29	24	21	19	21
	Fallow	1	33	26	25	23	19	19
		2	34	17	26	21	21	21
		3	34	22	23	22	20	25
	Plateau	1	17	17	15	11	8	8
		2	11	17	16	14	11	10
		3	15	20	21	14	13	12
South site	Millet	1	15	16	14	12	13	11
		2	21	17	14	18	17	14
		3	16	18	14	21	18	16
	Fallow	1	28	29	26	20	22	24
		2	16	29	24	23	26	27
		3	34	28	22	23	25	29
	Plataeu	1	14	11	10	9	11	10
		2	22	12	10	13	14	13
		3	14	13	10	13	15	14

* Number of misregistered columns.

5. Application to NOAA images

5.1. *NOAA data*

A total of 167 NOAA-AVHRR LAC images were obtained for the 1992 growing season (from 1 May to 25 October), for the area between latitude 11° and 16° N and longitude 0° and 5° E, centred around Niamey. All the images were mapped in a Plate Carrée projection. For each image, channels 1 (0·58–0·68 μm) and 2 (0·725–1·1 μm) were calibrated and atmospherically corrected (Ouaidrari *et al.* 1994). Unfortunately, the cloudiness is very important during this period, and only 16 clear images of the HAPEX-Sahel degree square have been retained for the whole growing season: Julian days 139, 163, 173, 174, 183, 190, 232, 239, 247, 262, 266, 271, 272, 287, 295, and 299. This temporal series is very irregular, and shows a gap of data in the middle of the growing season (between Julian days 190 and 232).

5.2. *Method*

The geometric registration between NOAA images and the vegetation map is made in three steps:

- Spatial degradation of the vegetation map at NOAA resolution (*cf* previous section).
- Autocorrelation between NOAA images and the vegetation map to identify the HAPEX-Sahel degree square on the NOAA images.
- Second-order polynomial geometric correction using ground control points (Niger River, plateau ...) identified on NOAA and the degraded vegetation map.

Once both images have been registered, one question remains: what is the optimal size of the blocks to take into account not only the misregistration between NOAA and the vegetation map (which has been studied previously), but also the heterogeneity of the radiometry of the components over the degree square? To answer this question, a second sensitivity analysis on the size of the blocks is done in real conditions. The results are illustrated by the coefficient of variation of the near-infrared reflectance of the components of CS and SS, on Julian day 262 (figure 9). On both sites, the coefficients of variation decrease down to a value of seven pixels of block size, and then increase slightly. That increase, not observed on the simulation,

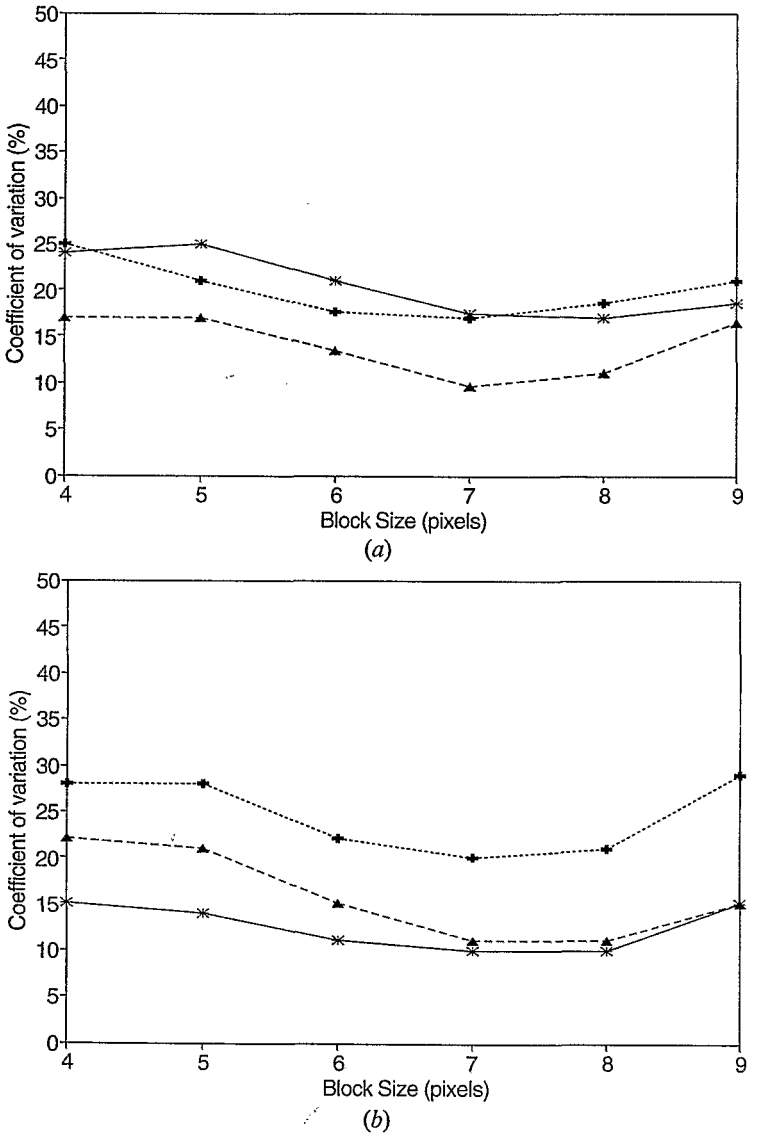

Figure 9. Coefficient of variation of the estimated near-infrared reflectances of millet (solid line), fallow (dotted line), and plateau (dashed line) components as function of the block size. Calculations were made for Julian day 262, on (*a*) Central, and (*b*) South sites.

can be explained by the variability of the spectral characteristics of a crop within a block. As the coefficient of variation is the only indicator on the 'quality' of the inversion, a mean block size of seven pixels has been chosen to inverse the mixture model over the satellite image.

5.3. *Results and discussion*

The previous methodology of signal deconvolution was applied to the 16 NOAA images. The seasonal profiles of the coefficient of variation calculated on CS and SS are presented for the millet in figures 10 (*a*) and (*b*) respectively. The other components

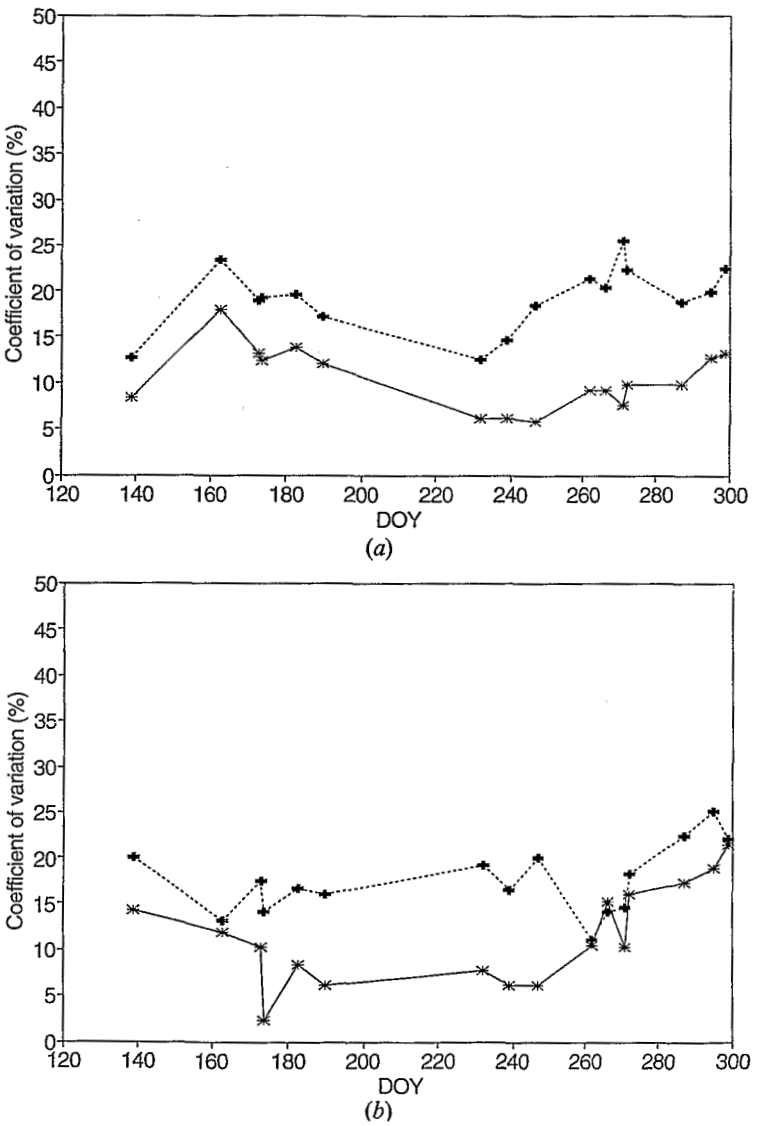

Figure 10. Coefficient of variation of millet red (solid line) and near-infrared (dotted line) reflectances throughout the growing season. Calculations were made with a block size of 7 pixels on the (*a*) Central, and (*b*) South sites.

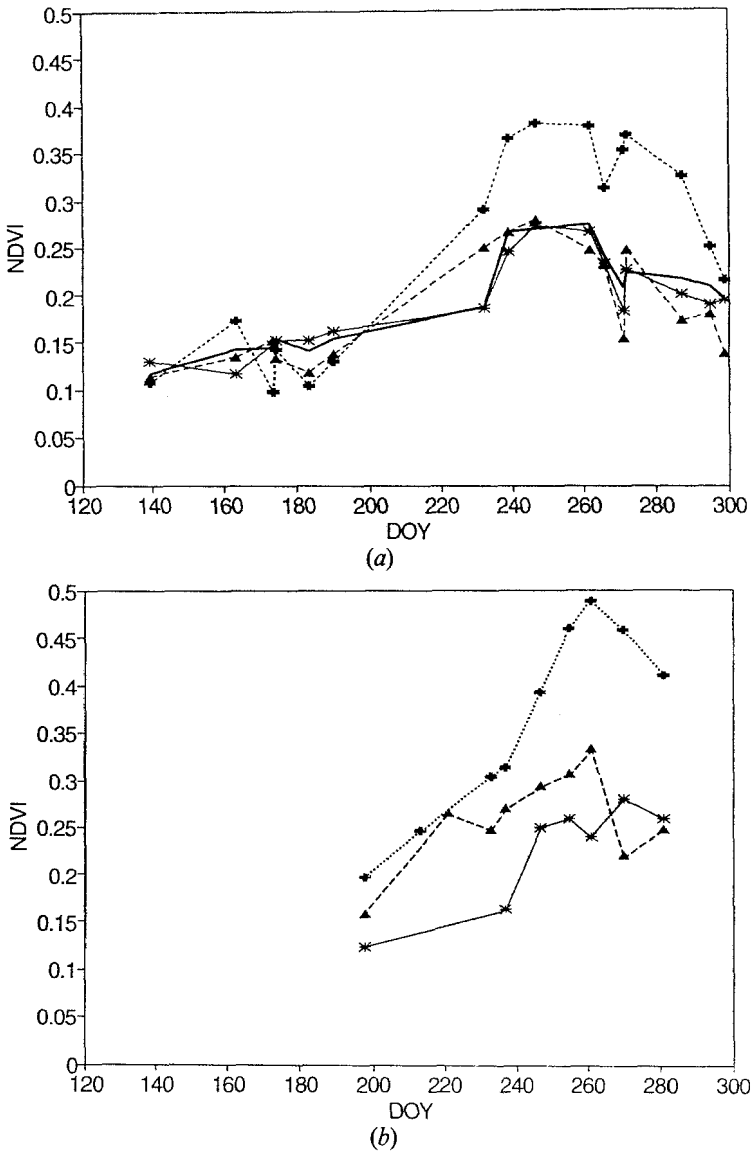

Figure 11. Central site NDVI profile of the millet (solid line), fallow (dotted line), and plateau (dashed line) components obtained from (*a*) deconvolution of the AVHRR signal, and (*b*) air-borne measurements. In (*a*) the bold line corresponds to the NDVI profile of the mixed AVHRR pixels.

have about the same profiles. The general trend is that the coefficients display a minimum in the middle of the growing season. Furthermore, at the beginning of the season, the coefficients of variation are smaller on SS than on CS. This could be explained by the rainfall regime, earlier on SS than on CS (Taupin *et al.* 1993), resulting in more homogeneous growth of the vegetation canopies. The coefficient of variation in the red channel is rather low (between 0 and 10 per cent in the middle of the rainy season), less than in the near-infrared channel (between 10 and 20 per cent at the same period).

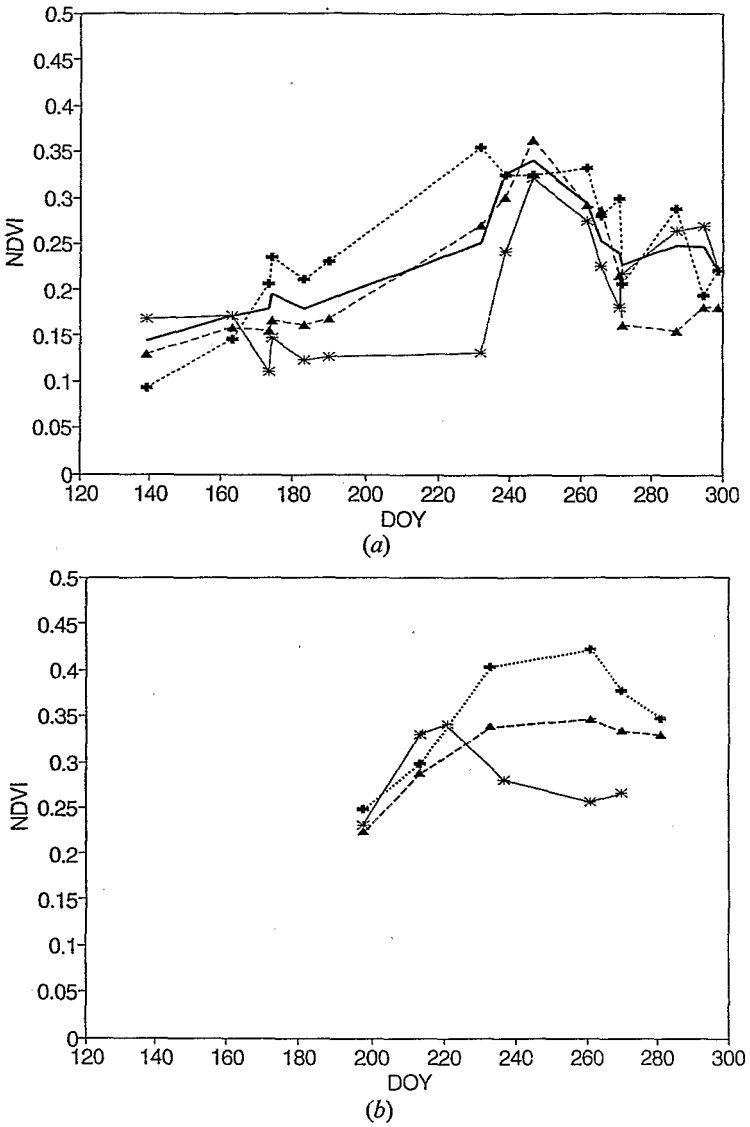

Figure 12. As figure 11 for the South site.

To test the methodology, the NDVI temporal profiles of the components on CS (figure 11 (*a*)) and SS (figure 12 (*a*)) are compared to the airborne NDVI acquired over the same sites (figures 11 (*b*) and 12 (*b*), respectively) during the HAPEX-Sahel field campaign (Hanan *et al.* 1996). The comparison cannot be quantitative because NOAA and TM channels are different and, above all, because the influence zone on NOAA images used in the calculations is about 533 km^2 (533 pixels), while the zone explored with the airborne radiometer is less than 1 km^2. Nevertheless, the shape of the profiles can be a good indicator of the quality of the method. On CS (figure 11), the NDVI profiles of each component are fairly well restituted. On both graphs, at the beginning of the growing period (Julian day 210) millet has the lower NDVI. During the growing period the NDVI of the fallow is well above the NDVI of the

other components. At the end, millet and fallow have about the same indices. The maxima of NDVI are reached at about the same time except for millet for which airborne measurements show a 'regrowth' at the end of the growing season. On SS (figure 12), the results are not as contrasted, and the comparison between measured and calculated NDVI is more difficult. Nevertheless, calculated fallow and plateau NDVI are almost confounded, which can be easily explained by the intermixing of these two classes in the region (presence of 'fallow' at the top of the plateau). The millet profile is completely different on both graph (maximum around Julian days 220 and 250 for measured and calculated reflectances respectively). To analyse the differences between the airborne and the satellite millet profiles, the seasonal profile of a NOAA pixel mainly composed of millet (82 per cent) and located close to the South site has been extracted and analysed. It displayed a maximum around Julian day 250, showing that the airborne measurements were not representative of the region. Even if the comparison must be done with caution because the airborne measurements cannot be representative of the components at NOAA scale, the results are encouraging on CS.

The difference between the two sites (earlier increase of the vegetation profiles on SS compared to CS) confirms the need of taking into account the spatial variability of the landscape components.

6. Summary and conclusions

As the signal of an AVHRR pixel is mostly a mixture of several component signals, linear mixture modelling appears to be a useful tool for image analysis. In the past years, this method has shown potential for ground cover estimates. This study shows potential for the restitution of the temporal and spatial variability of the spectral response of the landscape components. The methodology is based on the knowledge of the ground cover.

The linear mixture model was applied to a NOAA time series (1992) and a vegetation map issued from a SPOT image classification, over a HAPEX-Sahel degree square. This region is composed of a small number of vegetation types. The deconvolution of the signal was made over blocks of pixels to restrict the errors due to the misregistration between the vegetation map and NOAA images. Each block corresponds to a mixing equation, and the number of blocks equals the number of landscape components. The blocks were oriented perpendicularly to the vegetation gradient of the region to limit the variability of a component within the block of pixels. On a HAPEX-Sahel degree square, the sensitivity analysis showed that the optimal size of the blocks was 7×7 pixels. That means that the calculated spectral response of a component within a NOAA pixel is determined from the spectral response of the same component over an area of 41 km in the east–west direction and 13 km in the north–south direction. This size is large enough to smooth the fraction of soil coverage errors due to the misregistration, and small enough to have a limited reflectance variability due to the rainfall gradient.

The choice of the block size and its orientation depend on the scene. The orientation must be chosen according to information on the climatology, pedology, or on any domain contributing to the spatial variability of the spectral characteristics of the landscape components. The determination of the optimal block size is easy to calculate, and should constitute the first step of the methodology. But the strongest limitation of the method remains its sensitivity to the misregistration between NOAA images and the vegetation map. An analysis made on NOAA simulations has shown

that above one pixel of misregistration, the spectral response of the components was not correctly restituted. Furthermore, that sensitivity depends on the structure of the landscape. As expected, the method applied to a landscape made of small units will be less sensitive to the misregistration than if applied to a landscape with large and contrasted units. But, in the extreme case where all the units of landscape components are large, linear mixture modelling is not necessary to extract approximated pure spectral responses.

This methodology could have many applications in the future with the launch of SPOT4 (1997). In effect, the new instruments of this satellite will acquire simultaneously high spatial (HRVIR sensor) and temporal (Vegetation sensor) resolution images, reducing dramatically the misregistration between the two sources of information.

Acknowledgments

Financial support for HAPEX-Sahel was obtained from ORSTOM, Météo France, CNES, INSU/CNRS, Ministère de la Recherche et de l'Espace, Ministère de l'Environnement, Ministère de l'Education Nationale et de la Culture, and the Conseil Régional Midi-Pyrénées (France), ODA, NERC, the NERC TIGER programme, JEP (U.K.), NASA (U.S.A.), the European Community, and from several national funding agencies of Denmark, The Netherlands and Germany. Thanks to our collaborators in Niger at DMN, DRE, University of Niamey, INRAN, Aéroport de Niamey Authority, Groupement Aérien National, AGRHYMET, ICRISAT and ACMAD. H. Ouaidrari and A. Bégué were respectively supported by a French Government fellowship and CNES funding. Thanks to N. Hanan and S. Prince for providing the airborne measurements.

References

AGHRYMET, 1992, *Atlas agroclimatique des pays de la zone du CILSS-9: Cartes pluviométriques.* Published by CILSS, PNUD, OMM.

CHERCHALI, S. and FLOUZAT, G., 1994, Linear mixture modelling applied to AVHRR data for monitoring vegetation. *Proceedings of the International Geoscience and Remote Sensing Symposium (IGARSS'94), Pasadena, CA, 8–12 August 1994,* pp. 1242–1244.

CROSS, A., SETTLE, J., DRAKE, N. and PAIVINEN, R., 1991, Subpixel measurement of tropical forest cover using AVHRR data. *International Journal of Remote Sensing,* **12,** 1119–1129.

D'HERBES, J., COURAULT, D., TIMOUK, F., and VALENTIN, C., 1992, *Spatiocarte des états de surface, échelle 1/200 000. Programme HAPEX-Sahel et SALT* (Niamey: ORSTOM).

FISCHER, A., 1994, A model for the seasonal variation of vegetation index in coarse resolution data and its inversion to extract crop parameters. *Remote Sensing of Environment,* **48,** 220–237.

GOUTORBE, J., LEBEL, T., TINGA, A., BESSEMOULIN, P., BROUWER, J., DOLMAN, A., ENGMAN, E., GASH, J., HOEPFFNER, M., KABAT, P., KERR, Y., MONTENY, B., PRINCE, S., SAID, F., SELLERS, P., and WALLACE, J., 1994, HAPEX-Sahel: A large scale study of land-atmosphere interactions in the semi-arid tropics. *Annales Geophysicae,* **12,** 53–64.

GUÉRIF, M., DE BRISIS, S., and SEGUIN, B., 1991, Combined use of earth observation satellites and meteorological satellites for crop yield assessment in semiarid environments. *Proceedings of the 42nd Congress of the International Astronautical Federation, Montreal, Canada, 7–11 October 1991.*

HANAN, N., PRINCE, S., and HIERNAUX P. H. Y., 1991, Spectral modelling of multicomponent landscapes in the Sahel. *International Journal of Remote Sensing,* **12,** 1243–1258.

HANAN, N., BÉGUÉ, A., and PRINCE, S. D., 1996, Errors in remote sensing of intercepted photosynthetically active radiation: an example from HAPEX-Sahel. *Journal of Hydrology* (in press).

HOLBEN, B., and SHIMABUKURO, Y., 1993, Linear mixing model applied to coarse spatial resolution data from multispectral satellite sensors. *International Journal of Remote Sensing*, **14**, 2231–2240.

JUSTICE, C., (ed.) 1986, Special issue on monitoring the grasslands of semi-arid Africa using NOAA AVHRR data (editorial). *International Journal of Remote Sensing*.

JUSTICE, C., MARKHAM, B., TOWNSHEND, J., and KENNARD, R., 1989, Spatial degradation of satellite data. *International Journal of Remote Sensing*, **10**, 1539–1561.

KERDILES, H., and GRONDONA, M., 1995, NOAA-AVHRR NDVI decomposition and subpixel classification using linear mixing in the Argentinean Pampa. *International Journal of Remote Sensing*, **16**, 1303–1325.

LEBEL, T., SAUVAGEOT, H., HOEPFFNER, M., DESBOIS, M., GUILLOT, B., and HUBERT, P., 1992, Rainfall estimation in the Sahel: the EPSAT-NIGER experiment. *Hydrological Sciences Journal*, **37**, 201–215.

MALINGREAU, J., 1986, Global vegetation dynamics: satellite observations over Asia. *International Journal of Remote Sensing*, **7**, 1121–1146.

OLESON, K. W., SARLIN, S., GARRISON, J., SMITH, S., PRIVETTE, J. L. and EMERY, W. J., 1995, Unmixing multiple land-cover type reflectances from coarse spatial resolution satellite data. *Remote Sensing of Environment*, **54**, 98–112.

OUAIDRARI, H., IMBERNON, J. and DEDIEU, G., 1994, Use of a meteorology model to correct atmospheric effects in NOAA-AVHRR data. *International Journal of Remote Sensing*, **15**, 2257–2271.

PRINCE, S., KERR, Y., GOUTORBE, J., LEBEL, T., TINGA, A., BESSEMOULIN, P., BROUWER, J., DOLMAN, A., ENGMAN, E., GASH, J., HOEPFFNER, M., KABAT, P., MONTENY, B., SAID, F., SELLERS, P., and WALLACE, J., 1995, Geographical, biological and remote sensing aspects of the Hydrologic Atmospheric Pilot Experiment in the Sahel (HAPEX-Sahel). *Remote Sensing of Environment*, **51**, 215–234.

PUYOU-LASCASSIES, P., FLOUZAT, G., GAY, M., and VIGNOLLES, C., 1994, Validation of the use of multiple linear regression as a tool for unmixing coarse spatial resolution images. *Remote Sensing of Environment*, **49**, 155–166.

QUARMBY, N., TOWNSHEND, J., SETTLE, J., MILNES, M., HINDLE, T., and SILLEOS, N., 1992, Linear mixture modelling applied to AVHRR data for crop area estimation. *International Journal of Remote Sensing*, **13**, 415–425.

SMITH, M., ROBERTS, D., SHIPMAN, H., ADAMS, J., WILLIS, S., and GILLESPIE, A., 1987, Calibrating AIS images using the surface as a reference. *Proceedings of the 3rd Airborne Imaging Spectrometer Data Analysis Workshop* (Pasadena, CA: Jet Propulsion Laboratory), pp. 63–69.

TAUPIN, J., LEBEL, T., CAZENAVE, F., GRÉARD, M., KONG, J., LECOCQ, J., ADAMSON, M., D'AMATO, N., and MOHAMED, A. B., 1993, EPSAT-Niger, Campagne 1992. Technical Report, ORSTOM Niamey.

TUCKER, C., VANPRAET, C., SHARMAN, M., and ITTERSTUM, G. V., 1985, Satellite remote sensing of total herbaceous biomass production in the Senegalese Sahel: 1980–1984. *Remote Sensing of Environment*, **17**, 233–249.